Electrochimica Acta 142 (2014) 276–288

Contents lists available at ScienceDirect

Electrochimica Acta

journal homepage: www.elsevier.com/locate/electacta

Degradation of the azo dye Acid Red 1 by anodic oxidation and indirect electrochemical processes based on Fenton's reaction chemistry. Relationship between decolorization, mineralization and products

Xavier Florenza[a], Aline Maria Sales Solano[a,b,1], Francesc Centellas[a], Carlos Alberto Martínez-Huitle[b,1], Enric Brillas[a,1], Sergi Garcia-Segura[a,*]

[a] Laboratori d'Electroquímica dels Materials i del Medi Ambient, Departament de Química Física, Facultat de Química, Universitat de Barcelona, Martí i Franquès 1-11, 08028 Barcelona Spain

[b] Universidade Federal do Rio Grande do Norte, Centro de Ciências Exatas e da Terra, Instituto de Química, Lagoa Nova, CEP 59078-970, Natal Brazil

ARTICLE INFO

Article history:
Received 24 June 2014
Received in revised form 25 July 2014
Accepted 29 July 2014
Available online 7 August 2014

Keywords:
Acid Red 1
Anodic oxidation
Boron-doped diamond
Electro-Fenton
Photoelectro-Fenton

ABSTRACT

Solutions of 236 mg dm^{-3} Acid Red 1 (AR1), an azo dye widely used in textile dying industries, at pH 3.0 have been comparatively treated by anodic oxidation with electrogenerated H_2O_2 (AO-H_2O_2), electro-Fenton (EF) and photoelectro-Fenton (PEF) at constant current density (j). Assays were performed with a stirred tank reactor equipped with a Pt or boron-doped diamond (BDD) anode and an air-diffusion cathode for H_2O_2 generation from O_2 reduction. The main oxidizing agents were hydroxyl radicals produced at the anode from water oxidation in all methods and in the bulk from Fenton's reaction between generated H_2O_2 and 0.5 mmol dm^{-3} Fe^{2+} in EF and PEF. For each anode, higher oxidation power was found in the sequence AO-H_2O_2 < EF < PEF. The oxidation ability of the BDD anode was always superior to that of Pt. Faster and similar decolorization efficiency was achieved in EF and PEF owing to the quicker destruction of aromatics with hydroxyl radicals produced in the bulk. The PEF process with BDD was the most potent method yielding almost total mineralization due to the additional rapid photolysis of recalcitrant intermediates like Fe(III)-carboxylate complexes under UVA irradiation. The increase in j always enhanced the decolorization and mineralization processes because of the greater production of hydroxyl radicals, but decreases the mineralization current efficiency. A total of 11 aromatic intermediates, 15 hydroxylated compounds, 13 desulfonated derivatives and 7 short-linear carboxylic acids were identified. NH_4^+, NO_3^- and SO_4^{2-} ions were released during azo dye degradation. From the products detected, a comprehensive reaction sequence for AR1 mineralization is proposed. The relationship between decolorization, mineralization and products formed is finally discussed.

1. Introduction

Recently, the UNESCO's World Water Development Report [1] manifested the growing concern about dying industrial effluents. Large volumes of industrial effluents with high dye contents are discharged into water bodies causing esthetic problems derived from their color and their worrying hazardous effects on living beings. Azo dyes are the most used organic dyes, representing for over 70% of annual dyes consumption [2]. They have the azo group (–N=N–) as chromophore, associated with aromatic systems containing groups such as –OH and $-SO_3H$. Azo dyes are highly recalcitrant and are hardly removed by conventional biological and physicochemical methods, thus persisting in the aquatic environment [2,3]. They are toxic to aquatic organisms and humans [4,5] and possess carcinogenic, mutagenic and bactericide properties [1]. The development of powerful and effective oxidation processes to remove azo dyes and their by-products from wastewaters are required to avoid their adverse environmental impact and the danger they imply to public health.

Electrochemical advanced oxidation processes (EAOPs) are based on the *in situ* generation of hydroxyl radical (•OH) to mineralize organic matter in waters [6,7]. The high standard redox potential of this radical (E°(•OH/H_2O) = 2.80 V/SHE) favors its non-selective reaction with most organics giving dehydrogenated or

* Corresponding author. Tel.: +34 934021223; fax: +34 934021231.
E-mail addresses: sergigarcia@ub.edu, sergigs_87@hotmail.com (S. Garcia-Segura).
[1] ISE Active Member.

http://dx.doi.org/10.1016/j.electacta.2014.07.117
0013-4686/

hydroxylated derivatives up to complete combustion to CO_2, inorganic ions and water. EAOPs are promising and environmentally friendly technologies that are very effective for organics degradation and easily usable and scalable [6–10]. Although some papers have been recently published dealing with the decolorization and removal of several azo dyes by these methods [11–15], much deeper information about the influence of operating parameters and generated products on the degradation processes of a high number of these pollutants is needed to clarify the possible viability of EAOPs for wastewater remediation.

The most typical EAOP is anodic oxidation (AO), where adsorbed hydroxyl radical (M(•OH)) is generated from water discharge by reaction (1) at an anode (M) with high O_2-overpotential by applying a high current [6,13,16–20].

$$M + H_2O \rightarrow M(^{\bullet}OH) + H^+ + e^- \quad (1)$$

The non-active boron-doped diamond (BDD) anode is currently considered the best anodic material for AO since it generates very high amounts of reactive physisorbed BDD(•OH) radicals as a result of its very weak BDD-•OH interaction and great O_2-overpotential [21]. These properties confer BDD the ability of being more effective to remove aromatics including azo dyes than other common anodes such as Pt [22,23] and PbO_2 [24,25].

Carbonaceous cathodes like graphite [26], carbon or graphite felts [12,26–30], activated carbon fiber [31], carbon sponge [32], carbon-polytetrafluoroethylene (PTFE) gas (O_2 or air) diffusion [11,15,33–36], carbon nanotubes [37,38] and BDD [14,39,40] have shown a high efficiency for H_2O_2 electrogeneration from the two-electron reduction of injected O_2 from reaction (2):

$$O_2(g) + H^+ + 2e^- \rightarrow H_2O_2 \quad (2)$$

In an undivided cell for AO, the use of a carbon-PTFE air-diffusion cathode minimizes the possible cathodic reduction of organic pollutants [15,23]. In this EAOP, so-called AO with electrogenerated H_2O_2 (AO-H_2O_2), other weaker reactive oxygen species (ROS) than •OH can be produced at the anode, like hydroperoxyl radical ($HO_2^{\bullet}$) from H_2O_2 oxidation by reaction (3):

$$M + H_2O_2 \rightarrow M(HO_2^{\bullet}) + H^+ + e^- \quad (3)$$

Cathodes with ability for H_2O_2 electrogeneration have also been extensively used in indirect EAOPs based on Fenton's reaction chemistry [7–9]. The most common method is electro-Fenton (EF) [11,12,15,26–30,32,35,36], where •OH is produced in the bulk from the reaction between generated H_2O_2 and low amounts of added Fe^{2+} ion by Fenton's reaction (4) with optimum pH 2.8:

$$Fe^{2+} + H_2O_2 + H^+ \rightarrow Fe^{3+} + {}^{\bullet}OH + H_2O \quad (4)$$

Reaction (4) is catalytic and can be propagated from Fe^{2+} regeneration, pre-eminently by Fe^{3+} reduction at the cathode [27,32].

When an undivided cell is used in EF, organic molecules are mainly destroyed by the combined action of M(•OH) formed at the anode from reaction (1) and •OH produced in the bulk from reaction (4), along with a slower destruction by other weaker ROS such as H_2O_2 and $HO_2^{\bullet}$ [7]. Unfortunately, the EF treatment of aromatics with an air-diffusion cathode does not allow total mineralization of aromatic solutions due to the formation of Fe(III)-carboxylate complexes that are only slowly removed by BDD(•OH) [7,41]. This problem can be solved performing the photoelectro-Fenton (PEF) process, in which the solution treated by EF is irradiated with UVA light [15,31,33,42–45] and the degradation process is enhanced by: (i) the photoreduction of $Fe(OH)^{2+}$, the pre-eminent Fe^{3+} species at pH near 3, to regenerate Fe^{2+} producing more •OH from reaction (5) and (ii) the photolysis of generated Fe(III)-carboxylate complexes by the general reaction (6):

$$Fe(OH)^{2+} + h\nu \rightarrow Fe^{2+} + {}^{\bullet}OH \quad (5)$$

$$Fe(OOCR)^{2+} + h\nu \rightarrow Fe^{2+} + CO_2 + R^{\bullet} \quad (6)$$

The aim of this paper is to gain a better knowledge on the decolorization and mineralization processes of azo dyes during their EAOP treatments. To do this, the AO-H_2O_2, EF and PEF degradations of an azo dye widely used in the textile industry like Acid Red 1 (AR1, $C_{18}H_{13}N_3O_8S_2^{2-}$, see characteristics in Table 1) were comparatively studied at pH 3.0 using Pt/air-diffusion and BDD/air-diffusion cells. Solutions with 236 mg dm^{-3} AR1 (100 mg dm^{-3} of dissolved organic carbon (DOC)) were checked, since it corresponds to typical azo dye contents found in industrial effluents [34]. The influence of current density (j) on the decolorization efficiency and mineralization degree and rate was examined to better explain the role of generated oxidizing agents and/or UVA radiation in all the EAOPs tested. Aromatic intermediates were identified by liquid chromatography-mass spectrometry (LC-MS). Generated carboxylic acids and released inorganic ions were identified and quantified by high-performance liquid chromatography (HPLC). A reaction sequence for AR1 mineralization involving all the products detected is proposed. Finally, the relationship between decolorization, mineralization and products formed is discussed.

2. Experimental

2.1. Chemicals

Reagent grade Acid Red 1 was supplied by Sigma-Aldrich and used as received. Analytical grade anhydrous sodium sulfate and iron(II) sulfate heptahydrate were purchased from Fluka and Sigma-Aldrich, respectively. The solution pH was initially adjusted with analytical grade sulfuric acid supplied by Across Organics. Sodium perchlorate and perchloric acid, used in some trials, were analytical grade purchased from Merck. Carboxylic acids, other chemicals and solvents used in chromatographic techniques were of HPLC, LC-MS and analytical grade purchased from Sigma-Aldrich, Lancaster, Merck and Panreac. All solutions were prepared with high-purity water obtained from a Millipore Milli-Q system with resistivity > 18 MΩ cm at 25 °C.

2.2. Electrolytic system

Electrolytic experiments were performed in an open and undivided two-electrode cell of 150 cm^3 capacity with an external jacket allowing circulation of thermostated water regulated by a Selecta Digiterm 3000524 thermostat. The anode was a BDD thin film supplied by Adamant Technologies (La-Chaux-de-Fonds, Switzerland) or a Pt sheet of 99.99% purity supplied by SEMPSA (Barcelona, Spain). The cathode was a carbon-PTFE air-diffusion electrode from E-TEK (Somerset, NJ, USA), mounted as described elsewhere [46], allowing H_2O_2 generation from air injection at a flow rate of 300 cm^3 min^{-1}. All electrodes had a geometric area of 3 cm^2 and were separated about 1 cm. The assays were made at constant j by connecting the electrodes to an Amel 2053 potentiostat-galvanostat and the potential difference of the cell was directly measured with a Demestres 601BR digital multimeter. To remove the impurities of the BDD anode surface and activate the air-diffusion cathode before the degradation trials, they were polarized in 100 cm^3 of a 0.05 mol dm^{-3} Na_2SO_4 solution at 100 mA cm^{-2} for 180 min.

All experiments were carried out with 100 cm^3 of solutions containing 236 mg dm^{-3} AR1 in 0.05 mol dm^{-3} Na_2SO_4 as background electrolyte at pH 3.0. In EF and PEF, 0.5 mmol dm^{-3} Fe^{2+} were added to the solution as catalyst. The solution pH and the Fe^{2+} concentration were chosen since they have been found optimal for similar treatments of other aromatics [11,15,33–36]. The solution was maintained at 35.0 °C, which is the maximum temperature that our system can be thermostated without significant water

Table 1
Chemical structure and characteristics of Acid Red 1 azo dye.

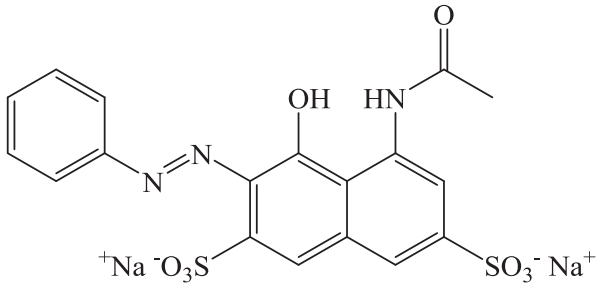

Azo form

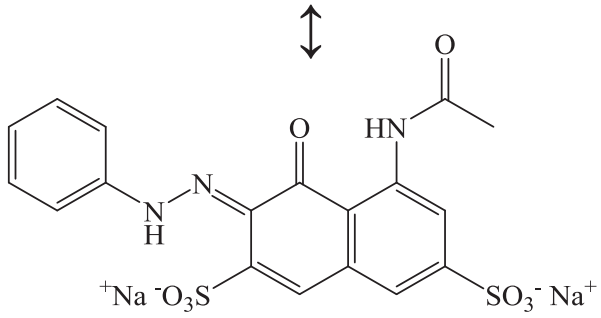

Hydrazone form

Chemical structure	
Chemical formula	$C_{18}H_{13}N_3Na_2O_8S_2$
IUPAC name	Sodium 5-(acetylamino)-4-hydroxy-3-(2-phenyldiazenyl)-2,7-naphthalenedisulfonate
Colour Index name	Acid Red 1
CAS number	3734-67-6
Colour Index number	18050
M [g mol^{-1}]	509.44
λ_{max} [nm]	506

evaporation during prolonged electrolysis time. The solution was stirred by a magnetic bar at 800 rpm to ensure homogeneity in solution and the mass transport of reactants toward/from the electrodes. A Philips 6-W black light blue tube lamp was used for UVA irradiation in PEF, providing wavelengths of 320-400 nm with λ_{max} = 360 nm with an energy of 5 W m^{-2}, as detected with a Kipp&Zonen CUV 5 global UV radiometer.

2.3. Instruments and analytical procedures

The solution pH was determined using a Crison GLP 22 pH-meter. Samples were collected at regular time intervals, alkalinized to stop the mineralization process and filtered with 0.45 μm PTFE filters purchased from Whatman before analysis. The decolorization of AR1 solutions was followed by monitoring their absorbance (A) decrease at the maximum visible wavelength of λ_{max} = 506 nm (see Table 1) using a Shimadzu 1800 UV-vis spectrophotometer thermostated at 35 °C to record the solution spectra between 200 and 800 nm. The percentage of color removal or decolorization efficiency was then calculated by Eq. (7) [2]:

$$\%\,\text{Color removal} = \frac{A_0 - A_t}{A_0} 100 \quad (7)$$

where A_0 and A_t are the absorbance at initial time and time t at λ_{max} = 506 nm, respectively.

The mineralization of AR1 solutions was monitored from their DOC abatement, determined on a Shimadzu VCSN Total Organic Carbon (TOC) analyzer. Reproducible DOC values with an accuracy of ±1% were obtained by injecting 50 μL aliquots into the analyzer. From the DOC decay, the mineralization current efficiency (MCE) for each trial was estimated by Eq. (8) [34]:

$$\text{MCE}\,(\%) = \frac{nFV_s\Delta(\text{DOC})_{exp}}{4.32 \times 10^7\, mIt} 100 \quad (8)$$

where F is the Faraday constant (96,487 C mol^{-1}), V_s is the solution volume (dm^3), $\Delta(\text{DOC})_{exp}$ is the experimental DOC decay (mg dm^{-3}), 4.32×10^7 is a conversion factor (3600 s h^{-1} × 12000 mg C mol^{-1}), m is the number of carbon atoms of AR1 (18 C atoms), I is the applied current (A), t is the electrolysis time (h) and n refers to the number of electrons involved in the total combustion of AR1 assuming the main formation of ammonium and sulfate ions from reaction (9):

$$C_{18}H_{13}N_3O_8S_2^{2-} + 36H_2O \rightarrow 18CO_2 + 2SO_4^{2-} + 3NH_4^+ + 73H^+ + 74e^- \quad (9)$$

Total nitrogen (TN) referred to all N-species present in solution was determined with a Shimadzu TNM-1 module coupled to the above TOC analyzer.

The evolution of generated carboxylic acids was followed by ion-exclusion HPLC using a Waters 600 LC fitted with a Bio-Rad Aminex HPX-87H, 300 mm × 7.8 mm (i.d.), column at 35 °C and coupled to a Waters 996 photodiode array detector set at λ = 210 nm. For this analysis, 20 μL aliquots were injected to the LC and a 4 mmol dm^{-3} H_2SO_4 at 0.6 cm^3 min^{-1} was used as mobile phase. Ammonium, nitrate and sulfate ions released during mineralization were analyzed by ion chromatography by injecting 25 μL aliquots

into a Shimadzu 10Avp LC coupled to a Shimadzu CDD 10Avp conductivity detector. The NH_4^+ concentration was determined using a Shodex IC YK-421, 125 mm × 4.6 mm (i.d.), cationic column at 40 °C and a 24.2 mmol dm^{-3} boric acid, 5.0 mmol dm^{-3} tartaric acid, 1.5 mmol dm^{-3} 18-crown-6 and 2.0 mmol dm^{-3} 2,6-pyridinedicarboxylic solution at 1.0 cm^3 min^{-1} as mobile phase. The NO_3^- and SO_4^{2-} contents were quantified with a Shim-Pack IC-A1S, 100 mm × 4.6 mm (i.d.), anionic column at 40 °C and circulating a mobile phase composed of 2.6 mmol dm^{-3} phthalic acid and 2.4 mmol dm^{-3} tris(hydroxymethyl)aminomethane (pH = 4.0) at 1.5 cm^3 min^{-1}.

Aromatic intermediates formed between 2 and 40 min of EF treatment of 100 cm^3 of 236 mg dm^{-3} AR1 solution in a BDD/air-diffusion cell at 33.3 mA cm^{-2} were identified by LC-MS using a Shimadzu SIL-20AC LC filled with a Teknokroma Mediterranea Sea C-18 3 μm, 15 mm × 0.46 mm (i.d.), column at 30 °C and coupled to a Shimadzu LCMS-2020 MS. The MS operated in negative mode with electrospray source ionization (ESI), by applying 4.5 kV interface voltage and 60 V Q-array RF voltage. The DL temperature was 250 °C and pure N_2 was used as nebulizing and dryer gas. Mass spectra were collected in the *m/z* range of 50-600 using both, total ion current (TIC) and selected ion (SIM) acquisition. This analysis was made by injecting 20 μL aliquots into the LC, previously filtered with a Millipore filter of 0.22 μm, using a 75:25 (v/v) acetonitrile/water (5 mmol dm^{-3} ammonium acetate) mixture at 0.2 cm^3 min^{-1} as mobile phase.

3. Results and discussion

3.1. Comparative degradation of Acid Red 1 by electrochemical advanced oxidation processes with a Pt or BDD anode

To assess the effectiveness of the EAOPs to degrade AR1, a first series of trials was made by treating 236 mg dm^{-3} azo dye solutions in 0.05 mol dm^{-3} Na_2SO_4 at pH 3.0 by AO-H_2O_2, EF and PEF using Pt/air-diffusion and BDD/air-diffusion cells at 100 mA cm^{-2} and 35 °C for 360 min. In these experiments, the solution pH remained practically unchanged, slowly decreasing up to final values of pH 2.7-2.8, probably due to the formation of acidic products like carboxylic acids [7,18].

Fig. 1a shows a very poor DOC removal of the AR1 solution by AO-H_2O_2 with Pt, only reaching 16% mineralization at the end of this treatment as a result of the low oxidation ability of Pt(•OH) formed from reaction (1) at the Pt surface, along with the poor oxidative action of other ROS like H_2O_2 and HO_2• generated from reactions (2) and (3). In contrast, the alternative use of a BDD anode causes a much faster DOC decay, up to attain 93% mineralization at 360 min. This positive degradation behavior can be related to the expected greater oxidation ability of generated BDD(•OH) at the BDD surface [6,24,25], indicating that it is the best anode to remove more rapidly and in larger extent the DOC of the AR1 solution comparatively with AO-H_2O_2.

Fig. 1a also highlights a remarkable effect of the anode material in the EF process. Thus, when Pt was used, DOC was rapidly reduced by 52% in 180 min, whereupon it was slightly removed. This enhancement in dye degradation compared to the AO-H_2O_2 process is due to the additional oxidation of organics by •OH produced in the bulk from Fenton's reaction (4). The very slow DOC removal found for EF with Pt at long electrolysis time suggests the formation of quite recalcitrant products that are difficultly destroyed by Pt(•OH) and •OH. The faster degradation process under the action of •OH in the bulk can also be observed in Fig. 1a for EF with BDD, primordially during the first 180 min of treatment where 80% DOC reduction was already achieved. At longer time, however, the degradation was progressively decelerated up to

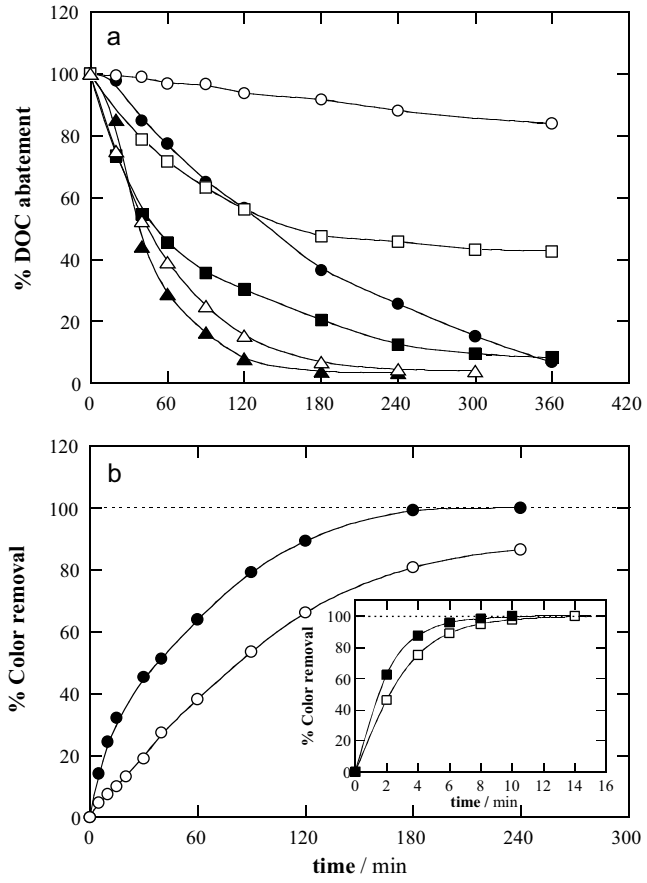

Fig. 1. Percentage of (a) DOC abatement and (b) color removal at λ_{max} = 506 nm vs. electrolysis time for the degradation of 100 cm^3 of 236 mg dm^{-3} Acid Red 1 (AR1) solutions in 0.05 mol dm^{-3} Na_2SO_4 at pH 3.0, 100 mA cm^{-2} and 35 °C using a (open symbols) Pt/air-diffusion or a (solid symbols) BDD/air-diffusion cell. Method: (○,●) Anodic oxidation with electrogenerated H_2O_2 (AO-H_2O_2), (□,■) electro-Fenton (EF) with 0.5 mmol dm^{-3} Fe^{2+} and (△,▲) photoelectro-Fenton (PEF) with 0.5 mmol dm^{-3} Fe^{2+} and 6 W UVA light of λ_{max} = 360 nm.

reaching 92% mineralization at 360 min, a value quite similar to 93% found for AO-H_2O_2 with BDD. These findings suggest the production of very recalcitrant products like Fe(III)-carboxylate complexes in EF, which are slowly removed mainly by BDD(•OH), thereby largely inhibiting the mineralization process at long electrolysis time [7,29,32]. When the PEF process was applied, less influence of the anode material was found due to the potent action of UVA irradiation, as can be seen in Fig. 1a. This EAOP yielded a very fast mineralization of the AR1 solution to yield almost total mineralization (> 96% DOC removal) after 300 min using Pt, and in a shorter time of 240 min for BDD. The large acceleration of the degradation in PEF compared to EF can then be related to the production of more amounts of •OH from reaction (5) along with the quick photolysis of intermediates like Fe(III)-carboxylate complexes via reaction (6) [35,36,41,42]. These phenomena are more significant when a Pt anode was used because the latter complexes are very slowly mineralized by Pt(•OH) and •OH, as stated above. The quicker removal of these compounds by BDD(•OH) can explain the superiority of PEF using BDD instead of Pt.

The role of the oxidizing agents generated in the comparative assays mentioned above to directly remove the azo dye was clarified by determining the decolorization efficiency of the treated solutions at λ_{max} = 506 nm. Note that the decolorization process could involve not only the cleavage of AR1 but also the destruction of other possible conjugated aromatic products that absorb at similar wavelength region, as found for other azo dyes [34,35]. Fig. 1b

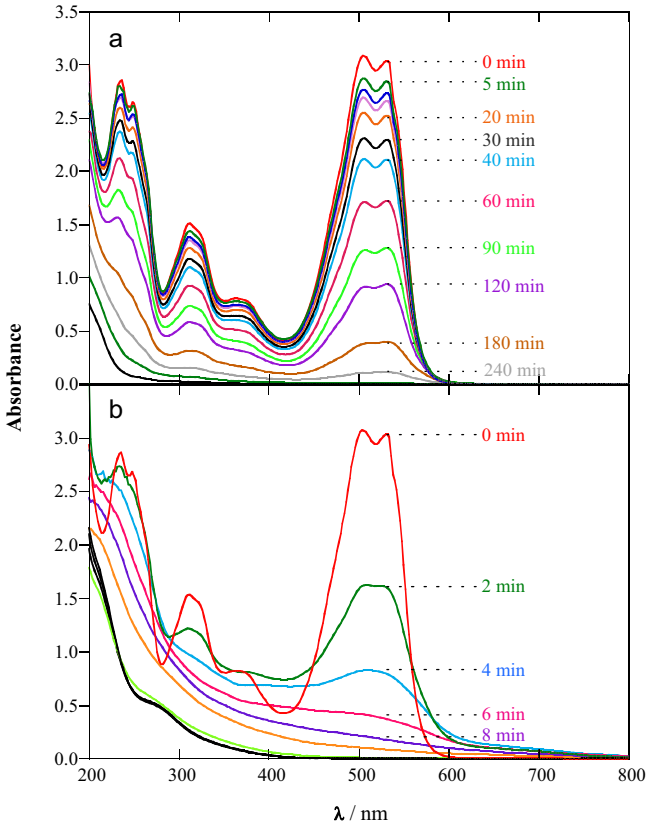

Fig. 2. Evolution of the UV-vis spectra recorded during the treatment of 100 cm^3 of 236 mg dm^{-3} AR1 solutions in 0.05 mol dm^{-3} Na_2SO_4 at pH 3.0 and 35 °C by (a) AO-H_2O_2 and (b) EF with 0.5 mmol dm^{-3} Fe^{2+} using a BDD/air-diffusion cell at 100 mA cm^{-2}.

shows that AO-H_2O_2 with BDD led to overall decolorization in about 240 min, time in which only 86% color removal was achieved using the Pt anode. This corroborates the existence of a fast attack of BDD(•OH) on AR1, which becomes much slower under the action of Pt(•OH) as expected from its lower oxidation ability. In contrast, the inset panel of Fig. 1b depicts a much quicker decolorization under EF conditions, which was completely attained after ca. 14 min for Pt and only 10 min for BDD. This behavior is indicative of the predominant destruction of AR1 by •OH formed from Fenton's reaction (4), suggesting the pre-eminent destruction of aromatic intermediates by this oxidant. The slightly higher color removal reached in EF using BDD instead of Pt can be justified again by the quicker parallel attack of BDD(•OH) than Pt(•OH), although the reactivity of both radicals over the azo dye is much smaller than •OH. These results evidence the different reactivity of hydroxyl radicals generated in the bulk by Fenton's reaction and those formed at the anode surface from water oxidation. It is noteworthy that the percentage of color removal-time plots for the PEF processes with Pt and BDD (data not shown) overlapped with the corresponding EF ones. This evidences low production of additional •OH induced from photolytic reaction (5) and high stability of AR1 under UVA illumination.

Figs. 2a and 2b show the evolution of the UV-vis spectra recorded in the above AO-H_2O_2 and EF treatments, both with BDD, respectively. The spectrum of the starting solution displayed a visible band with two strong peaks centered at 506 nm (characteristic of AR1, see Table 1) and 530 nm. According to the behavior of other azo dyes [47], these bands can be associated with two tautomeric forms in equilibrium given in Table 1, the azo form with λ_{max} = 506 nm and the hydrazone one with λ = 530 nm, where the hydroxyl group appears as carbonyl group and its hydrogen is linked to the azo group. A similar absorbance can be observed for both peaks, suggesting near 50% of each tautomeric form. In addition, the UV region exhibited three bands, the weakest one at 364 nm corresponding to the amide group linked to the naphthalene ring, other band centered at 312 nm related to the naphthalenic ring and the most intense one associated with the benzenic ring at 236 nm. As can be seen in Fig. 2a, the intensity of all the bands of AR1 decayed at similar rate with prolonging the AO-H_2O_2 treatment up to 240 min. This indicates that the azo dye is the principal species present in the solution during the decolorization process, suggesting that its aromatics products are rapidly removed by BDD(•OH). Note also the very low absorption intensity between 200 and 400 nm at 240 min of electrolysis, as expected if small quantities of aliphatic products like carboxylic acids are accumulated in the medium because they are destroyed at similar rate as produced. For the EF treatment, however, Fig. 2b shows a rapid drop in intensity of all the bands disappearing at 6 min of electrolysis, although a wide undefined band remained in the visible region up to 10 min. This behavior can be accounted for the generation of some colored aromatic intermediates while solution is decolorized, which are completely destroyed by •OH in 10 min. At this time, an intense absorption in the UV region of 200-400 nm can be observed, suggesting the accumulation of large quantities of aliphatic products that are destroyed more slowly and pre-eminently by BDD(•OH), in agreement with the slow DOC fall found in EF (see Fig. 1a).

3.2. *Effect of current density on the electrochemical advanced oxidation processes with BDD*

The current density is an operating variable that influences the amount of oxidizing hydroxyl radicals generated in EAOPs. To clarify the effect of this parameter on AR1 degradation, the above 236 mg dm^{-3} azo dye solutions were treated by the methods tested between 16.7 and 100 mA cm^{-2} using the BDD/air-diffusion cell, which comparatively yielded the most potent procedures.

Figs. 3a, 3b and 3c depict a gradual increase in DOC removal with increasing *j* for AO-H_2O_2, EF and PEF, respectively. After 360 min of the former treatment, Fig. 3a shows that mineralization rose from 54% for 16.7 mA cm^{-2} to 93% for 100 mA cm^{-2}, as expected from the concomitant increase in rate of reaction (1) yielding more amounts of BDD(•OH) that accelerate the degradation process. For the comparative EF processes, Fig. 3b depicts an enhancement of the mineralization rate due to the acceleration of reaction (2) yielding more H_2O_2 and hence higher quantities of •OH from Fenton's reaction (4). Thus, DOC was reduced by 68% and 92% at the end of the electrolyses at 16.7 and 100 mA cm^{-2}, respectively. The faster DOC removal was always achieved by the most potent PEF process, where the time needed for reaching almost total mineralization decreased from 360 min at 16.7 mA cm^{-2} to 240 min at 100 mA cm^{-2} (see Fig. 3c). This trend can be explained by the quicker photolysis of intermediates by UVA light since they are more rapidly formed by the greater amounts of BDD(•OH) and •OH produced at higher *j*.

Figs. 4a, 4b and 4c present the MCE values calculated from Eq. (8) for the trials of Figs. 3a,3b and 3c, respectively. The efficiency increased progressively with decreasing *j* in all cases, becoming greater in the sequence AO-H_2O_2 < EF < PEF, in agreement with their relative oxidation ability over AR1. Thus, these processes yielded maximum MCE values of 12%, 32% and 39% at the lowest *j* of 16.7 mA cm^{-2}. Note that the efficiency did not vary significantly during each AO-H_2O_2 treatment, suggesting a practically constant destruction rate of intermediates with BDD(•OH), according to the evolution of the UV-vis spectra shown in Fig. 2a. In contrast, the MCE values underwent a dramatic decay at long electrolysis time of EF and PEF, corroborating the formation of more recalcitrant products like Fe(III)-carboxylate complexes at the beginning of both treatments, in agreement to the UV-vis spectra of Fig. 2b. These

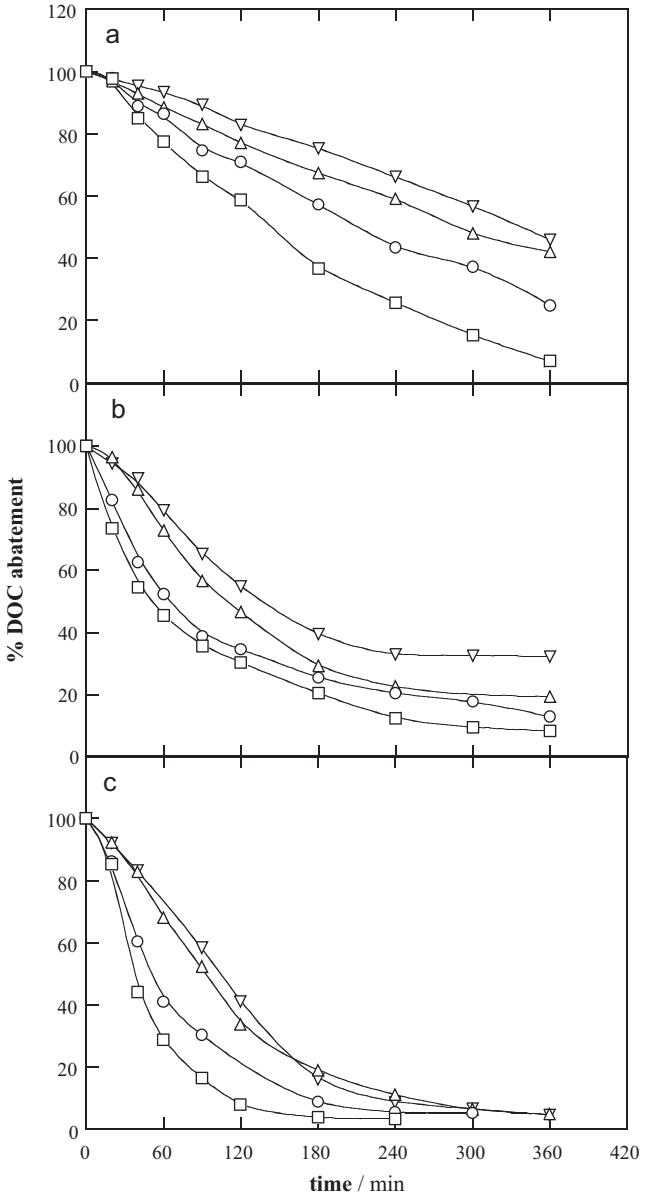

Fig. 3. Effect of current density on the change of per cent of DOC abatement with electrolysis time for 100 cm^3 of 236 mg dm^{-3} AR1 solutions in 0.05 mol dm^{-3} Na_2SO_4 at pH 3.0 and 35 °C treated by (a) AO-H_2O_2, (b) EF and (c) PEF using a BDD/air-diffusion cell. In the two latter methods, 0.5 mmol dm^{-3} Fe^{2+} was added to the solution. Applied *j*: (▽) 16.7 mA cm^{-2}, (△) 33.3 mA cm^{-2}, (○) 66.7 mA cm^{-2} and (□) 100 mA cm^{-2}.

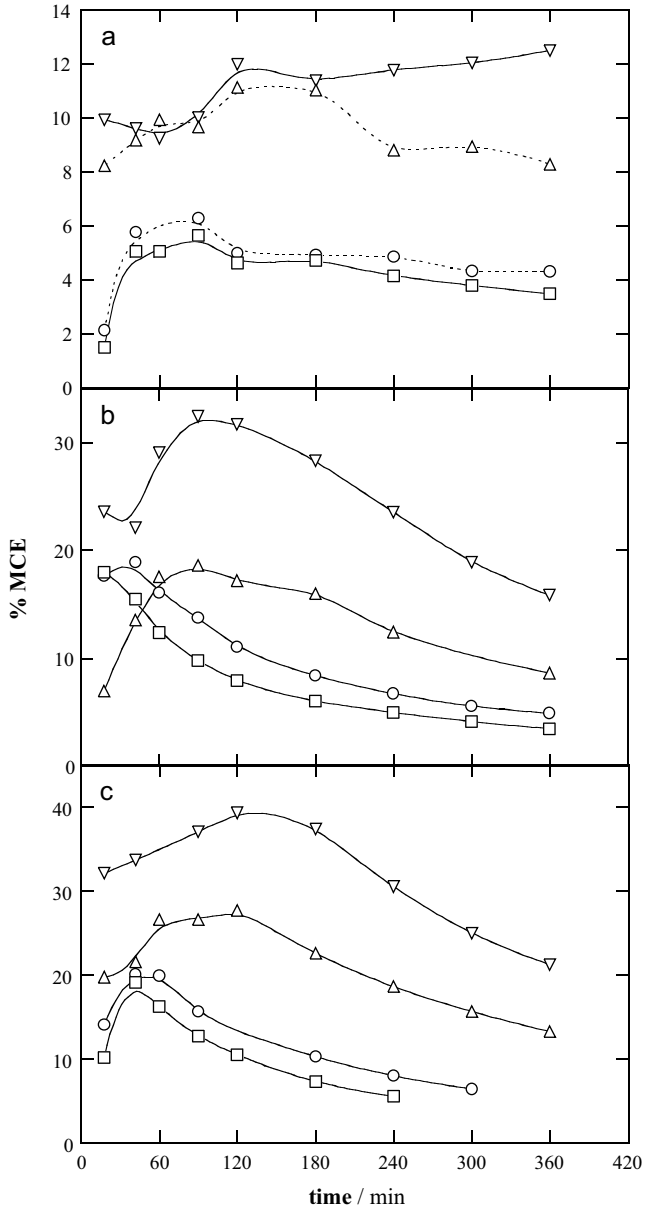

Fig. 4. Mineralization current efficiency vs. electrolysis time for the trials of Fig. 3.

species are then more slowly destroyed by the oxidizing species generated and/or photolyzed by UVA light, thereby making the process less efficient. On the other hand, the rise in MCE at lower *j* for all the EAOPs seems contradictory to the decay in DOC abatement shown in Fig. 3. This opposite tendency can be related to a gradual loss in the relative production of hydroxyl radicals due to the acceleration of their non-oxidizing reactions with the increase of *j*, which causes fewer attacks on organic compounds, thus reducing the efficiency. These parasitic reactions involve primordially the oxidation of BDD(•OH) to O_2 at the anode by reaction (10), as well as the reaction of •OH in the bulk with generated H_2O_2 to form $HO_2^•$ via reaction (11) and with Fe^{2+} by reaction (12) [6–8]:

$$BDD(^•OH) \rightarrow 2BDD + O_2 + 2H^+ + 2e^- \quad (10)$$

$$H_2O_2 + {}^•OH \rightarrow HO_2^• + H_2O \quad (11)$$

$$Fe^{2+} + {}^•OH \rightarrow Fe^{3+} + OH^- \quad (12)$$

The positive effect of increasing *j* on the decolorization efficiency of the above trials was also found. As can be seen in Fig. 5a, a rise in *j* from 33.3 to 100 mA cm^{-2} promoted the production of BDD(•OH) in AO-H_2O_2, enhancing the destruction of AR1 and hence, favoring the decolorization process. Total decolorization was achieved at about 300 and 240 min for 66.7 and 100 mA cm^{-2}, respectively, needing a much longer time for lower *j* values. Fig. 5b highlights that times of 40, 20 and 10 min were needed for reaching total decolorization at 33.3, 66.7 and 100 mA cm^{-2}, respectively, of EF. This trend can be related to the enhancement of •OH formed from Fenton's reaction (4) because of the acceleration of H_2O_2 production from reaction (2). Similar results were obtained for PEF, corroborating the small participation of reaction (5) in •OH generation.

The decolorization rate related to the change of the absorbance at λ = 506 nm with time was analyzed for each trial from kinetic equations with simple reaction orders. Excellent straight lines were obtained for a pseudo-first-order reaction, as presented in the inset panels of Fig. 5a and 5b. Note that the decolorization rate cannot

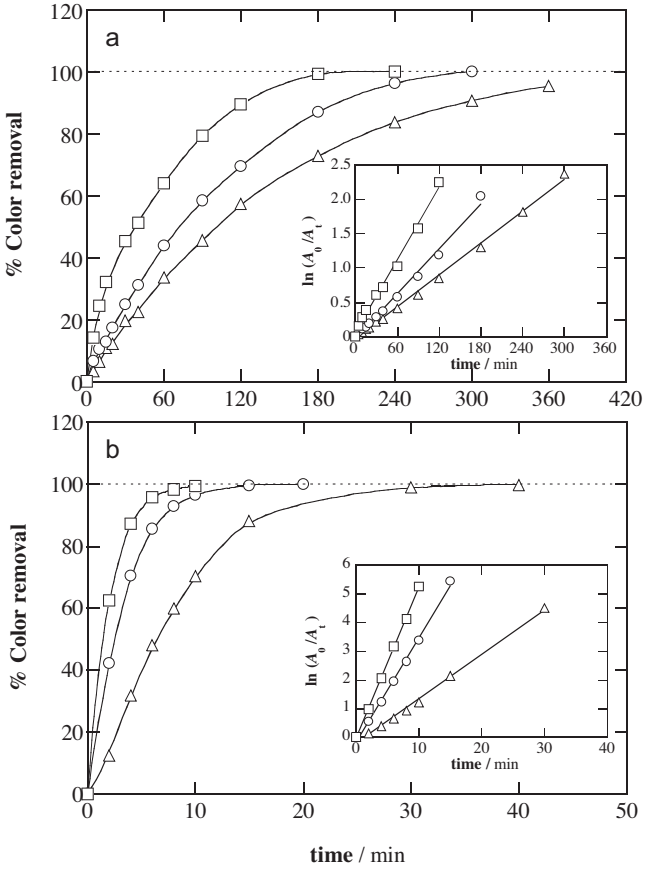

Fig. 5. Influence of current density on the variation of decolorization efficiency with electrolysis time for the degradation of 100 cm^3 of 236 mg dm^{-3} AR1 solutions in 0.05 mol dm^{-3} Na_2SO_4 at pH 3.0 and 35 °C by (a) AO-H_2O_2 and (b) EF with 0.5 mmol dm^{-3} using a BDD/air-diffusion cell. Applied *j*: (△) 33.3 mA cm^{-2}, (○) 66.7 mA cm^{-2} and (□) 100 mA cm^{-2}. The inset panels show the corresponding kinetic analysis considering a pseudo-first-order decay for the dye absorbance at λ_{max} = 506 nm.

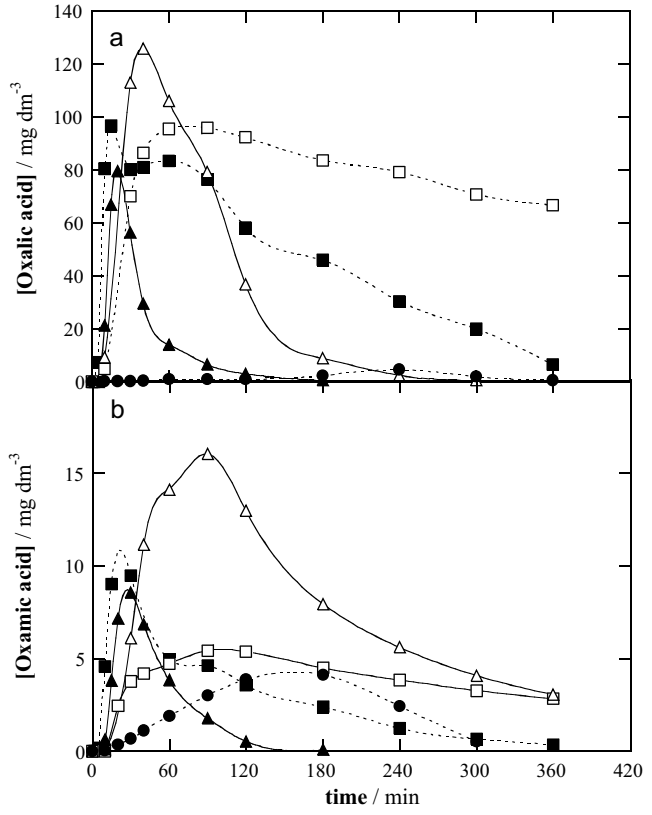

Fig. 6. Evolution of (a) oxalic and (b) oxamic acids detected during the treatment of 100 cm^3 of 236 mg dm^{-3} AR1 solutions in 0.05 mol dm^{-3} Na_2SO_4 at pH 3.0 and 35 °C by (●) AO-H_2O_2, (□,■) EF with 0.5 mmol dm^{-3} Fe^{2+} and (△,▲) PEF with 0.5 mmol dm^{-3} Fe^{2+} using a: (open symbols) Pt/air-diffusion or (solid symbols) BDD/air-diffusion cell at 100 mA cm^{-2}.

be strictly associated with the decay kinetics of AR1 due to the formation of colored aromatic intermediates, as deduced from the UV-vis spectra recorded in EF (see Fig. 2b). Thus, the apparent rate constant (k_{dec}) derived from the above analysis has only experimental validity. Increasing k_{dec} values of 1.3×10^{-4} s^{-1} (R^2 = 0.997), 1.8×10^{-4} s^{-1} (R^2 = 0.991) and 2.9×10^{-4} s^{-1} (R^2 = 0.993) for AO-H_2O_2 and 2.6×10^{-3} s^{-1} (R^2 = 0.992), 6.1×10^{-3} s^{-1} (R^2 = 0.994) and 8.8×10^{-3} s^{-1} (R^2 = 0.999) for EF were determined at 33.3, 66.7 and 100 mA cm^{-2}, respectively. These findings demonstrate that the k_{dec} values for EF and PEF are about 20-30 times higher than those of AO-H_2O_2, corroborating the predominant role of generated •OH in the bulk to remove aromatics in the indirect electrochemical processes based on Fenton's reaction chemistry.

3.3. *Identification of aromatic intermediates and evolution of generated carboxylic acids*

Table 2 collects the aromatic products detected by LC-MS during the first 40 min of EF treatment of a 236 mg dm^{-3} azo dye solution at 33.3 mA cm^{-2}, i.e., while it is decolorized. Since organics are mainly attacked by hydroxyl radicals, the same kinds of products are expected in AO-H_2O_2 and PEF. As can be seen, apart from the starting compound (**1**), 11 aromatic intermediates, 15 hydroxylated derivatives and 13 desulfonated compounds were identified by this technique. The aromatic intermediates include molecules with similar structure to the azo dye (compounds **2**-**4**), as well as naphthalenic (compounds **5**-**8**) and benzenic (compounds **9**-**12**) derivatives coming from the loss or oxidation of functional groups. Acetamide (**13**) and aniline (**14**), expected to be released from these degradation reactions, were not detected by LC-MS.

The further destruction of the above aromatic products is expected to yield short-chain carboxylic acids [7,8]. This point was confirmed by analyzing the solutions treated at 100 mA cm^{-2} by ion-exclusion HPLC. These chromatograms revealed the formation of succinic (**15**, t_r = 11.75 min), maleic (**16**, t_r = 8.24 min), acetic (**17**, t_r = 14.9 min), glycolic (**18**, t_r =12.2), oxamic (**19**, t_r = 9.4 min), oxalic (**20**, t_r = 6.9 min) and formic (**21**, t_r = 13.7 min) acids. Acids **15**-**18** are expected to be formed from the cleavage of the benzene moieties, which are then oxidized to acids **20** and **21** [7,15,23,32–36]. Acid **19** could be formed from the degradation of **13** [48]. Note that acids **19**-**21** are ultimate intermediates that are directly transformed into CO_2 [41,44].

Ion-exclusion chromatograms of the solutions electrolyzed by AO-H_2O_2 with Pt did not exhibit any carboxylic acid due to the low oxidation ability of Pt(•OH), giving small mineralization at 360 min (see Fig. 1a). In contrast, when a BDD anode, with much higher oxidation ability, was used maximum contents of 10.5 mg dm^{-3} for **18**, 8.0 mg dm^{-3} for **17**, 4.6 mg dm^{-3} for **20** (see Fig. 6a), 4.1 mg dm^{-3} for **19** (see Fig. 6b) and 1.2 mg dm^{-3} for **21**, along with traces (< 1.0 mg dm^{-3}) of **15** and **16**, were found. All these acids were practically removed at the end of the treatment, only corresponding to about 10% of the 7.0 mg dm^{-3} DOC of the final solution (see Fig. 1a). This means that small amounts of other persistent products that react even more hardly with BDD(•OH) than carboxylic acids are formed during AR1 degradation.

A different pattern was found for the EF and PEF treatments, where acids **15**-**18** and **21** were accumulated at short electrolysis

Table 2
Aromatic compounds along with their hydroxylated and desulfonated derivatives identified by LC-MS during the EF treatment of 100 cm^3 of 236 mg dm^{-3} AR1 solution using a BDD/air-diffusion cell at 33.3 mA cm^{-2}.

Number	Name	Molecular formula	Hydroxylated derivatives			Desulfonated derivatives
			Number of -OH added	*m/z*	Number of $-SO_3^-$ lost	*m/z*
1	Acid Red 1 (5-Acetylamino-4-hydroxy-3-phenylazo-naphthalene-2,7-disulfonate)	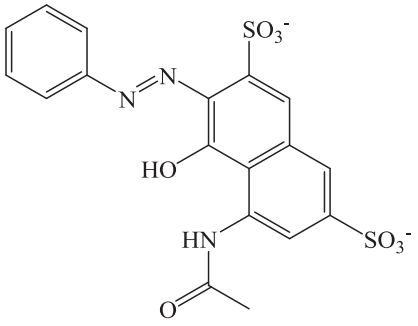	-	232[b]	1	1 400[a]
			1	240[b]	1	
2	5-Amino-4-hydroxy-3-phenylazo-naphthalene-2,7-disulfonate	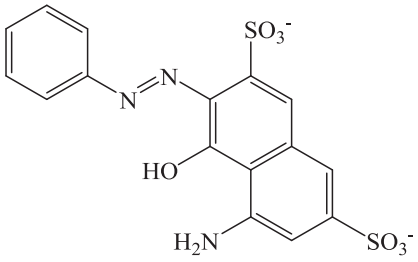	-	211[b]		
			1	219[b]		
			2	227[b]		
3	4-Hydroxy-5-nitro-3-phenylazo-naphthalene-2,7-disulfonate	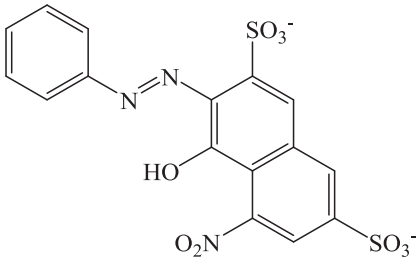	-	226[b]		1 388[a]
			1	234[b]	1	
4	4-Hydroxy-3-phenylazo-naphthalene-2,7-disulfonate	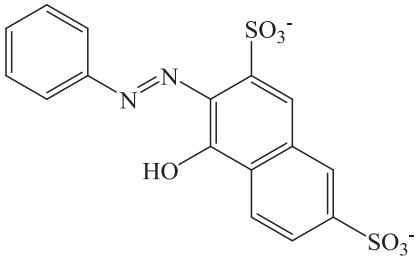	-	407[a]	1	1 327[a]
			1	211[b]		
			2	219[b]		
5	5-Acetylamino-3-amino-4-hydroxy-naphthalene-2,7-disulfonate	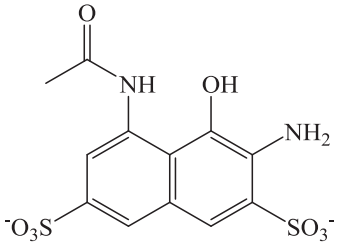	-	187[b]	1	1 295[a]
			1	195[b]	1	1 311[a]
			2	203[b]	1	1 327[a]
			3	211[b]	1	1 343[a]

Table 2 (*Continued*)

Number	Name	Molecular formula	Hydroxylated derivatives			Desulfonated derivatives
			Number of -OH added	*m/z*	Number of $-SO_3^-$ lost	*m/z*
6	4-Acetylamino-5-hydroxy-naphthalene-2,7-disulfonate	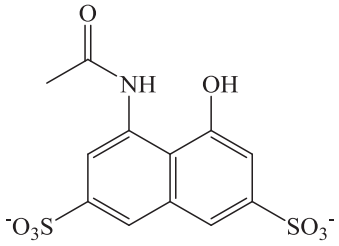	-	180[b]		2 232[a]
			1	376[a]		1 328[a]
			2	392[a]	2	
			3	408[a]	1	
7	4-Hydroxy-3,5-dinitro-naphthalene-2,7-disulfonate	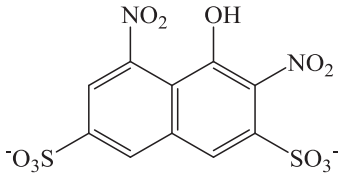	-	-[c]	2	2 233[a]
			1	409[a]	1	1 329[a]
			2	425[a]		
			3	441[a]		
8	4-Amino-5-hydroxy-naphthalene-2,7-disulfonate	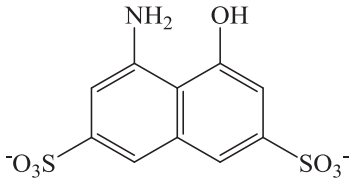	-	159[b]		2 190[a]
			2	-[c]	2	
9	3-Hydroxy-5-sulfophthalic acid	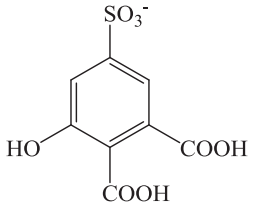	-	261[a]		1 197[a]
			1	138[b]	1	
10	4-Amino-3,6-dihydroxy-5-sulfophthalic acid	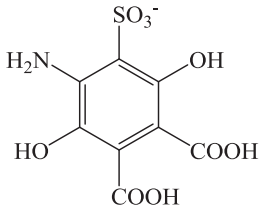	1	292[a]		
11	Hydroxy-3-acetylamino-benzenesulfonate	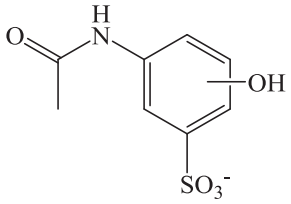	1	232[a]		
12	Aminophenol	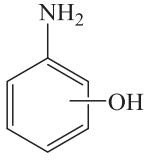	3	156		

Negative ion with *z* = [a] 1 and [b] 2
[c] Not detected

times up to 4 mg dm^{-3} as maximal and their Fe(III) complexes disappeared in about 40-60 min owing to the action of BDD(•OH), •OH and/or UVA light. However, these species acted much more slowly over the Fe(III) complexes of acids **19** and **20**, which were accumulated in large extent and persisted during long electrolysis times. Fig. 6a shows a quick accumulation of acid **20** up to near 80-120 mg dm^{-3} in both EF and PEF processes. This acid was slowly reduced to 67 mg dm^{-3} after 360 min of EF with Pt because of the low reactivity of Pt(•OH) and •OH to destroy Fe(III)-oxalate species, whereas it was removed up to 7 mg dm^{-3} in EF with BDD as a result of the quicker attack of BDD(•OH) on such complexes. The predominant photolysis of Fe(III)-oxalate complexes under UVA irradiation via reaction (6) explains the total disappearance of acid **20** at 300 min of PEF with Pt, which was even shortened to 180 min using BDD by their parallel destruction with BDD(•OH). A similar behavior can be observed in Fig. 6b for the evolution of acid **19**, accumulated in much lesser extent. For EF, the maximum content of 5.4 mg dm^{-3} attained by this acid at 90-120 min using Pt decayed to a final value of 2.8 mg dm^{-3} because of the low removal power of Pt(•OH) and •OH on Fe(III)-oxamate complexes, whereas using BDD these species were totally destroyed by the more potent action of BDD(•OH). In PEF with Pt much more quantity of acid **19** was accumulated (16 mg dm^{-3}), suggesting that UVA light promotes the degradation of *N*-derivatives, and it was rapidly reduced to a final content of 3.0 mg dm^{-3} due to the photolysis of Fe(III)-oxamate complexes. The combined action of BDD(•OH) and UV light caused the total disappearance of these species in only 180 min using PEF with BDD.

A mass balance of the final content of both acids **19** and **20** revealed their contribution in only 18.7, 1.9 and 0.8 mg dm^{-3} to the 42.3, 8.3 and 4.0 mg dm^{-3} DOC of the final solutions of EF with Pt, EF with BDD and PEF with Pt, respectively (see Fig. 1a). These findings, along with the absence of carboxylic acids in the final solution of PEF with BDD with 3.3 mg dm^{-3} DOC, indicate the formation of other persistent products that are hardly removed by hydroxyl radicals and UVA light.

3.4. Time-course of released inorganic ions

To assess the evolution of inorganic ions like NH_4^+, NO_3^- and SO_4^{2-} expected from the degradation of AR1, 236 mg dm^{-3} azo dye solutions were treated by AO-H_2O_2, EF and PEF with BDD using 0.05 mol dm^{-3} $NaClO_4$ at pH 3.0 regulated with $HClO_4$ at 100 mA cm^{-2} for 360 min. The corresponding DOC-time plots found in this perchlorate medium were quite similar to those previously described for 0.05 M Na_2SO_4 in Fig. 1a; the former medium was then preferred for a better measurement of the concentration of released SO_4^{2-} ion. Moreover, the TN of final solutions was determined to quantify the remaining soluble N.

After 360 min of AO-H_2O_2, Figs. 7a and 7b highlight the accumulation of 1.9 mg dm^{-3} NH_4^+ (7.6% of initial N) and 19.1 mg dm^{-3} NO_3^- (22.0% of initial N). The sum of both species and the N of acid **19** contained in the remaining solution (see Fig. 6b) only yielded 29.8% of initial N, very far from 93% determined from TN. This means that the final solution with 7.0 mg dm^{-3} DOC is primordially composed of other unidentified *N*-products of low molecular mass and low carbon content. In contrast, Figs. 7a and 7b reveal the superiority of N loss as NH_4^+ compared to NO_3^- in EF and PEF. At the end of the former process, 8.3 mg dm^{-3} NH_4^+ (32.0% of initial N) and 14.1 mg dm^{-3} NO_3^- (16.5% of initial N) were found, whereas the latter one yielded 5.5 mg dm^{-3} NH_4^+ (22.0% of initial N) and 9.2 mg dm^{-3} NO_3^- (10.5% of initial N). The TN of both final solutions corresponded to 60.0% of initial N, a value superior to 48.5% and 32.5% obtained as sum of the released inorganic ions in EF and PEF, respectively. This indicates again the presence of

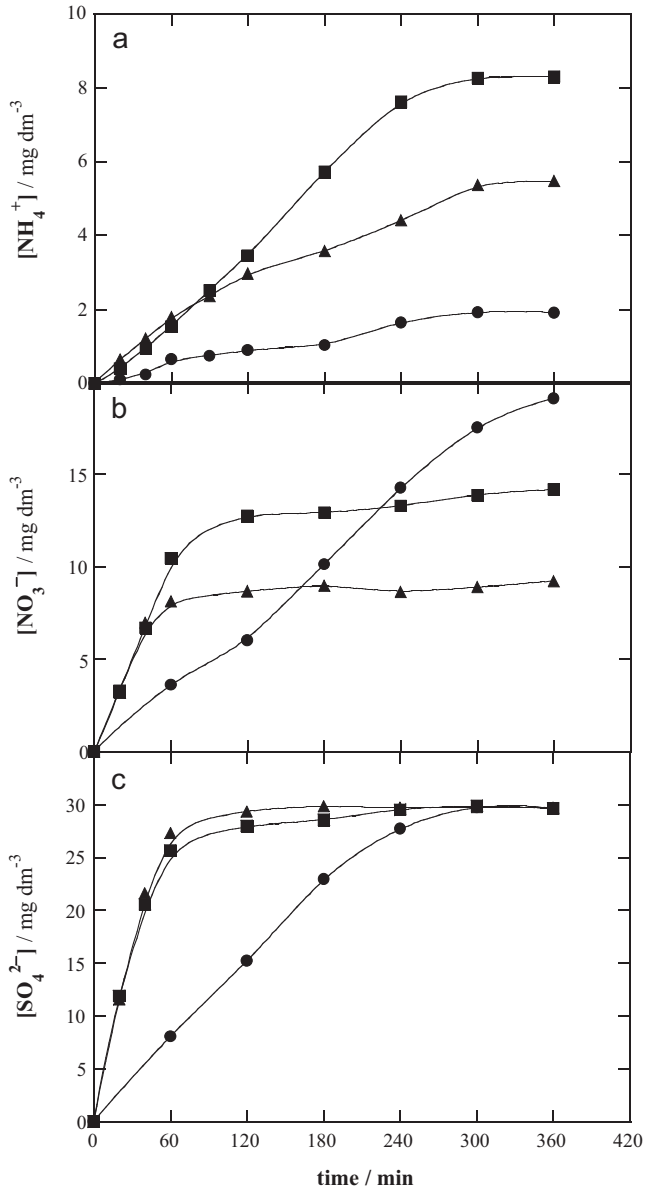

Fig. 7. Evolution of (a) ammonium, (b) nitrate and (c) sulfate ions detected during the degradation of 100 cm^3 of 236 mg dm^{-3} AR1 solutions in 0.05 mol dm^{-3} $NaClO_4$ at pH 3.0 and 35 °C using a BDD/air-diffusion cell at 100 mA cm^{-2}. Method: (●) AO-H_2O_2, (■) EF with 0.5 mmol dm^{-3} Fe^{2+} and (▲) PEF with 0.5 mmol dm^{-3} Fe^{2+}.

a large proportion of unidentified *N*-recalcitrant products in their final solutions. It is remarkable that the continuous oxidation with BDD(•OH) favors the preponderance of N lost as NO_3^- in AO-H_2O_2, whereas •OH and UVA light promote the release of N as NH_4^+ in EF and PEF. Moreover, the action of •OH and UVA light in the latter two processes leads to the loss of a larger proportion of initial N (about 40%) from the solution, probably in the form of N_2 and N_xO_y species.

Fig. 7c shows the evolution of SO_4^{2-} ion released from the sulfonic groups of the azo dye. While this ion was continuously accumulated for 300 min in AO-H_2O_2, it was released throughout less time, in about 120-180 min, and in a similar way by EF and PEF, suggesting that •OH rather than BDD(•OH) favors the desulfonation reactions of intermediates. In all these treatments, a final SO_4^{2-} content of 29.6 mg dm^{-3} corresponding to 100% of initial S was obtained, thereby corroborating that the two sulfonic groups of AR1 are completely released as SO_4^{2-} ion.

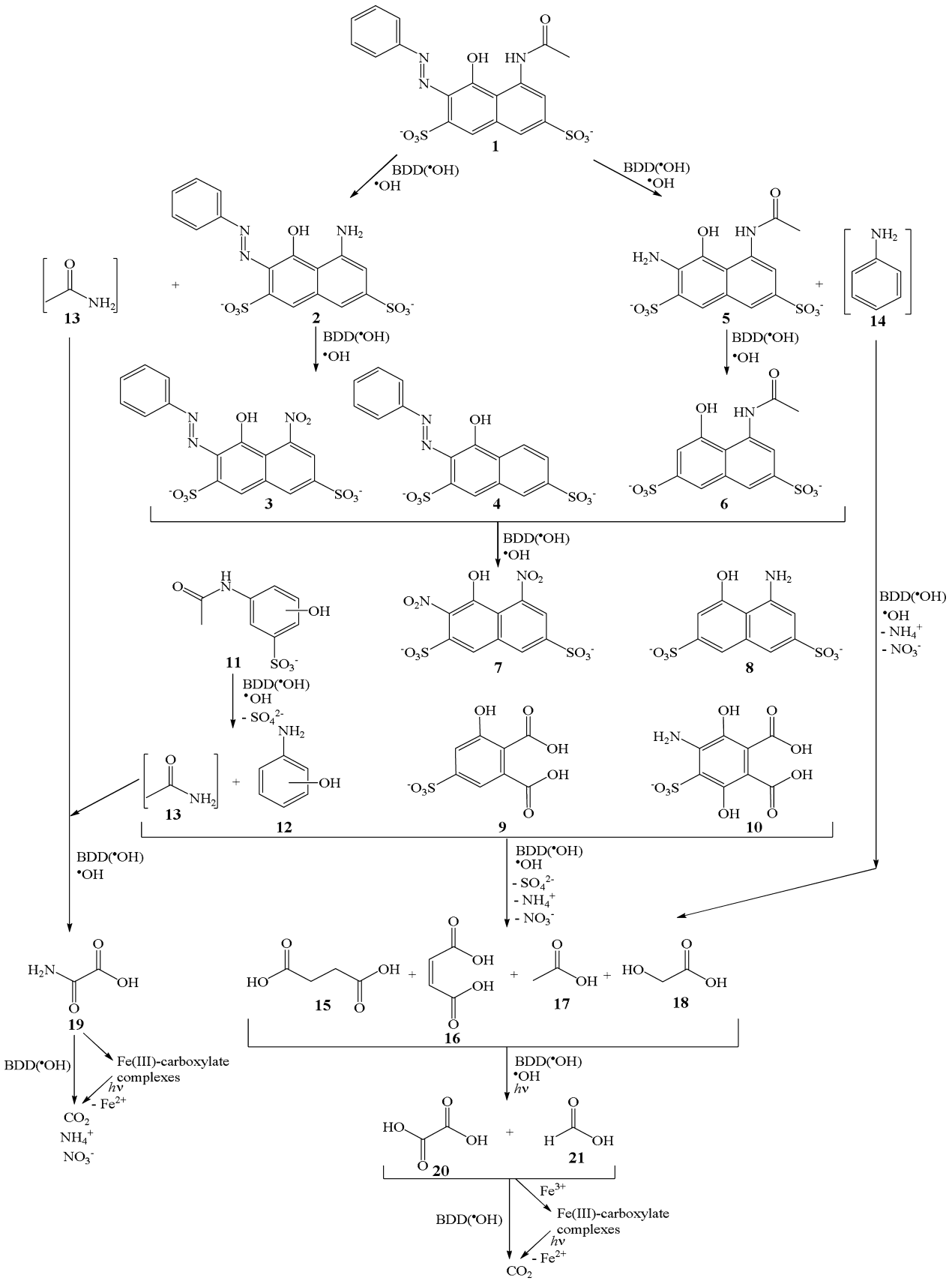

Fig. 8. Proposed reaction sequence for the mineralization of Acid Red 1 in acidic medium by AO-H_2O_2, EF and PEF with a BDD anode. The compounds in parentheses are hypothesized.

3.5. Proposed reaction pathway for Acid Red 1 mineralization

Based on the main intermediates detected in the BDD/air-diffusion cell, Fig. 8 presents a reaction sequence proposed for AR1 mineralization in acidic medium by all the EAOPs with BDD. While all compounds can be always oxidized by BDD(•OH), •OH is considered as the main oxidant of aromatics in EF and PEF. Their hydroxylated and desulfonated derivatives are not specified for simplification. In EF and PEF, Fe(III)-carboxylate species are always formed, only being detailed for acids **19**-**21**. Parallel slower reactions with other weaker ROS (H_2O_2 and HO_2•) are also feasible.

The sequence is initiated by the oxidation of **1** to yield either the compound **2** with release of **13** or the cleavage of the azo bond to produce the naphthalenic compound **5** losing **14**. Further degradation of **2** leads to the nitro-compound **3** or its deaminated compound **4**, whereas the subsequent deamination of **5** gives the compound **6**. The oxidation of **3**, **4** and **6** yields the naphthalenic derivatives **7** and **8**, the phthalic acid compounds **9** and **10** and the benzenesulfonic acid **11**, which is converted into the aminophenol **12** with loss of **13**. The cleavage of the benzenic ring of compounds **9**, **10**, **12** and **14** leads to a mixture of acids **15**-**18**, which are finally converted into the acids **20** and **21**. Parallel oxidation of **13** gives the acid **19**. The ultimate acids **19**-**21** can then be slowly mineralized with BDD(•OH) in AO-H_2O_2, whereas their Fe(III) complexes can be slowly destroyed primordially with BDD(•OH) in EF, but quickly photolyzed by UVA light in PEF. NH_4^+, NO_3^- and SO_4^{2-} ions are released during the deamination, denitration and desulfonation reactions, respectively, involved in the degradation process.

3.6. Relationship between decolorization, mineralization and generated products

The above findings indicate a close relationship between decolorization, mineralization and accumulation of products for AR1 degradation. The slow decolorization found by AO-H_2O_2 due to the slow cleavage of the azo bond suggests a higher recalcitrant character of AR1 than its aromatic products, which are poorly accumulated as deduced from the UV-vis spectra shown in Fig. 2a. Results of Fig. 1a highlights that AR1 mineralization in AO-H_2O_2 is enhanced when decolorization and, consequently, destruction of aromatic intermediates are already significant, which makes more effective the attack of BDD(•OH) to mineralize the generated short-linear aliphatic compounds like carboxylic acids. In the indirect electrochemical methods based on the Fenton's reaction chemistry, the more potent action of •OH in the bulk favors both the decolorization and mineralization at the starting steps, as can be seen in Figs. 1a and 1b, leading to a much higher accumulation of intermediates during their degradation processes. The UV-vis spectra recorded in Fig. 2b during the EF treatment suggests the accumulation of colored aromatic products, identified as compounds **2**-**4** together their hydroxylated and desulfonated derivatives by LC-MS (see Table 2). These colored oxidation products are also expected in AO-H_2O_2, but their low concentration in the medium does not affect significantly the shape of the peaks in its UV-vis spectra. A significant decolorization is also needed in EF and PEF to begin an effective mineralization, primordially at the lowest *j* values where less amounts of oxidant BDD(•OH) and •OH are generated, as deduced from Figs. 3b and 5b. The recalcitrant character of final Fe(III)-carboxylate complexes can be clearly observed at long electrolysis time in EF, which caused a dramatic fall in MCE. The quick photodecarboxylacion of such complexes, along with the photolysis of other intermediates, explains that PEF is the most powerful EAOP for AR1 mineralization. Inorganic ions are usually released at the beginning of all process, with pre-eminent loss of the initial N as NO_3^- ion in AO-H_2O_2 and as NH_4^+ ion in EF and PEF. This points again to the lower oxidation ability of BDD(•OH) than •OH over the aromatic products generated. However, persistent *N*-derivatives of low molecular mass are always formed avoiding the total mineralization of AR1.

4. Conclusions

The effectiveness of EAOPs using a Pt or BDD anode and an air-diffusion cathode to degrade AR1 has been corroborated in terms of the decolorization efficiency and mineralization rate at pH 3.0. The oxidation power of these methods increased in the sequence AO-H_2O_2 < EF < PEF regardless of the anode used. This behavior is explained by the quicker oxidation of aromatic pollutants with •OH in the bulk in the two latter methods than with M(•OH) formed at the corresponding anode surface. The use of a BDD anode compared to Pt always yielded faster decolorization and higher mineralization rate, because of the superior oxidation power of BDD(•OH) than Pt(•OH). Faster and similar decolorization efficiency was found for both EF and PEF processes due to the high photostability of AR1 under UVA irradiation. The UV-vis spectra of their electrolyzed solutions with BDD showed the formation of colored aromatic intermediates, which were detected by LC-MS. Almost total mineralization was only achieved in PEF due to the rapid photolysis of persistent intermediates like Fe(III)-carboxylate complexes. The increase in *j* always enhanced the decolorization and mineralization processes because of the greater production of BDD(•OH) and •OH, but the concomitant increase in rate of the parasitic reactions of these radicals decreased the mineralization current efficiency. Under all experimental conditions, the PEF process with BDD was the most powerful EAOP for AR1 degradation. However, the degradation kinetics of real dying effluents could be enhanced and be more cost-effective by using sunlight as inexpensive and renewable energy source, with high irradiation intensity and a wider applicable range of wavelengths than artificial UVA light [15]. A total of 11 aromatic intermediates, 15 hydroxylated compounds and 13 desulfonated derivatives were identified by LC-MS and 7 short-linear carboxylic acids were detected and quantified by ion-exclusion HPLC. While all the initial S of AR1 was converted into SO_4^{2-} ion, the initial N was mineralized preferentially as NO_3^- ion in AO-H_2O_2 and as NH_4^+ ion in EF and PEF. A large loss of N from solution was found for the two latter methods and the formation of very persistent *N*-derivatives of low molecular mass prevented reaching total mineralization in PEF. A reaction sequence involving all the products detected is proposed for AR1 mineralization by the EAOPs with BDD. The relationship between decolorization, mineralization and products formed during azo dye degradation is finally discussed.

Acknowledgements

The authors thank financial support from MICINN (Ministerio de Ciencia e Innovación, Spain) under the project CTQ2010-16164/BQU, co-financed with FEDER funds. A.M.S. Solano acknowledges her Doctoral fellowships from CAPES and CNPq (doutorado sanduíche under the program Ciências sem fronteiras). S. Garcia-Segura thanks the Doctoral grant awarded from MEC (Ministerio de Educación y Ciencia, Spain).

References

[1] UNESCO, The United Nations World Water Decelopment Report 4, Volume 1: Managing Water Report under Uncertainty and Risk, 2012.
[2] C.A. Martínez-Huitle, E. Brillas, Decontamination of wastewaters containing synthetic organic dyes by electrochemical methods: A general review, Appl. Catal. B: Environ. 87 (2009) 105.
[3] T. Robinson, G. McMullan, R. Marchant, P. Nigam, Remediation of dyes in textile effluent: a critical review on current treatment technologies with a proposed alternative, Biores. Technol. 77 (2001) 247.

[4] K.P. Sharma, S. Sharma, S. Sharma, P.K. Singh, S. Kumar, R. Grover, P.K. Sharma, A comparative study on characterization of textile wastewaters (untreated and treated) toxicity by chemical and biological tests, Chemosphere 69 (2007) 48.
[5] S.M.A.G. Ulson de Souza, E. Forgiarini, A.A. Ulson de Souza, Toxicity of textile dyes and their degradation by the enzyme horseradish peroxidase (HRP), J. Hazard. Mater. 147 (2007) 1073.
[6] M. Panizza, G. Cerisola, Direct and mediated anodic oxidation of organic pollutants, Chem. Rev. 109 (2009) 6541.
[7] E. Brillas, I. Sirés, M.A. Oturan, Electro-Fenton process and related electrochemical technologies based on Fenton's reaction chemistry, Chem. Rev. 109 (2009) 6570.
[8] I. Sirés, E. Brillas, Remediation of water pollution caused by pharmaceutical residues based on electrochemical separation and degradation technologies: A review, Environ. Int. 40 (2012) 212.
[9] L. Feng, E.D. van Hullebusch, M.A. Rodrigo, G. Esposito, M.A. Oturan, Removal of residual anti-inflammatory and analgesic pharmaceuticals from aqueous systems by electrochemical advanced oxidation processes. A review, Chem. Eng. J. 228 (2013) 944.
[10] G.R. de Oliveira, C.K.C. de Araújo, C.A. Martínez-Huitle, D.R. da Silva, Complementary mechanism model for the electrochemical mineralization, Curr. Org. Chem. 16 (2012) 1957.
[11] S. Garcia-Segura, F. Centellas, C. Arias, J.A. Garrido, R.M. Rodríguez, P.L. Cabot, E. Brillas, Comparative decolorization of monoazo, diazo and triazo dyes by electro-Fenton process, Electrochim Acta 58 (2011) 303.
[12] M. Panizza, M.A. Oturan, Degradation of Alizarin Red by electro-Fenton process using a graphite-felt cathode, Electrochim. Acta 56 (2011) 7084.
[13] M.G. Tavares, L.V.A. da Silva, A.M.S. Solano, J. Tonholo, C.A. Martínez-Huitle, C.L.P.S. Zanta, Electrochemical oxidation of Methyl Red using $Ti/Ru_{0.3}Ti_{0.7}O_2$ and Ti/Pt anodes, Chem. Eng. J. 204-206 (2012) 141.
[14] C. Ramírez, A. Saldaña, B. Hernández, R. Acero, R. Guerra, S. Garcia-Segura, E. Brillas, J.M. Peralta-Hernández, Electrochemical oxidation of methyl orange azo dye at pilot flow plant using BDD technology, J. Ind. Eng. Chem. 19 (2013) 571.
[15] F.C. Moreira, S. Garcia-Segura, V.J.P. Vilar, R.A.R. Boaventura, E. Brillas, Decolorization and mineralization of Sunset Yellow FCF azo dye by anodic oxidation, electro-Fenton, UVA photoelectro-Fenton and solar photoelectro-Fenton processes, Appl. Catal. B: Environ. 142-143 (2013) 877.
[16] M. Panizza, A. Kapalka, Ch. Comninellis, Oxidation of organic pollutants on BDD anodes using modulated current electrolysis, Electrochim. Acta 53 (2008) 2289.
[17] M.A. Rodrigo, P. Cañizares, A. Sánchez-Carretero, C. Sáez, Use of conductive-diamond electrochemical oxidation for wastewater treatment, Catal. Today 151 (2010) 173.
[18] E. Brillas, S. Garcia-Segura, M. Skoumal, C. Arias, Electrochemical incineration of diclofenac in neutral aqueous medium by anodic oxidation using Pt and boron-doped diamond anodes, Chemosphere 79 (2010) 605.
[19] E. Tsantaki, T. Velegraki, A. Katsaounis, D. Mantzavinos, Anodic oxidation of textile dyehouse effluents on boron-doped diamond electrode, J. Hazard. Mater. 207-208 (2012) 91.
[20] M.B. Ferreira, J.H.B. Rocha, J.V. de Melo, C.A. Martinez-Huitle, M.A. Quiroz Alfaro, Use of a dual arrangement of flow cells for electrochemical decontamination of aqueous solutions containing synthetic dyes, Electrocatalysis 4 (2013) 274.
[21] A. Kapalka, G. Fóti, C. Comninellis, Kinetic modeling of the electrochemical mineralization of organic pollutants for wastewater treatment, J. Appl. Electrochem. 38 (2008) 7.
[22] M. Hamza, R. Abdelhedi, E. Brillas, I. Sirés, Comparative electrochemical degradation of the triphenylmethane dye Methyl Violet with boron-doped diamond and Pt anodes, J. Electroanal. Chem. 627 (2009) 41.
[23] E.B. Cavalcanti, S. Garcia-Segura, F. Centellas, E. Brillas, Electrochemical incineration of omeprazole in neutral aqueous medium using a platinum or boron-doped diamond. Degradation kinetics and oxidation products, Water Res. 47 (2013) 1803.
[24] L. Ciríaco, C. Anjo, J. Correia, M.J. Pacheco, A. Lopes, Electrochemical degradation of ibuprofen on $Ti/Pt/PbO_2$ and Si/BDD electrodes, Electrochim. Acta 54 (2009) 1464.
[25] C. Flox, C. Arias, E. Brillas, A. Savall, K. Groenen-Serrano, Electrochemical incineration of cresols: A comparative study between PbO_2 and boron-doped diamond anodes, Chemosphere 74 (2009) 1340.
[26] E. Rosales, M. Pazos, M.A. Longo, M.A. Sanromán, Electro-Fenton decoloration of dyes in a continuous reactor: A promising technology in colored wastewater treatment, Chem. Eng. J. 155 (2009) 62.
[27] A. Özcan, M.A. Oturan, N. Oturan, Y. Şahin, Removal of Acid Orange 7 from water by electrochemically generated Fenton's reagent, J. Hazard. Mater. 163 (2009) 1213.
[28] A. Dhaouadi, N. Adhoum, Degradation of paraquat herbicide by electrochemical advanced oxidation methods, J. Electroanal. Chem. 637 (2009) 33.
[29] N. Oturan, E. Brillas, M.A. Oturan, Unprecedent total mineralization of atrazine and cyanuric acid by anodic oxidation and electro-Fenton with a boron-doped diamond anode, Environ. Chem. Lett. 10 (2012) 165.
[30] F.E.F. Rêgo, A.M.S. Solano, I.C. da Costa Soares, D.R. da Silva, C.A. Martínez-Huitle, M. Panizza, Application of electro-Fenton process as alternative for degradation of Novacron Blue dye, J. Environ. Chem. Eng. 2 (2014) 875.
[31] A. Wang, J. Qu, H. Liu, J. Ru, Mineralization of an azo dye Acid Red 14 by photoelectro-Fenton process using an activated carbon fiber cathode, Appl. Catal. B: Environ. 84 (2008) 393.
[32] A. Özcan, Y. Sahin, A.S. Koparal, M.A. Oturan, Carbon sponge as a new cathode material for the electro-Fenton process. Comparison with carbon felt cathode and application to degradation of synthetic dye Basic Blue 3 in aqueous medium, J. Electroanal. Chem. 616 (2008) 71.
[33] C. Flox, P.L. Cabot, F. Centellas, J.A. Garrido, R.M. Rodríguez, C. Arias, E. Brillas, Solar photoelectro-Fenton degradation of cresols using a flow reactor with a boron-doped diamond anode, Appl. Catal. B: Environ. 75 (2007) 17.
[34] E.J. Ruiz, A. Hernández-Ramírez, J.M. Peralta-Hernández, C. Arias, E. Brillas, Application of solar photoelectro-Fenton technology to azo dyes mineralization: Effect of current density, Fe^{2+} and dye concentration, Chem. Eng. J. 171 (2011) 385.
[35] S. Garcia-Segura, A. El-Ghenymy, F. Centellas, R.M. Rodríguez, C. Arias, J.A. Garrido, P.L. Cabot, E. Brillas, Comparative degradation of the diazo dye Direct Yellow 4 by electro-Fenton, photoelectro-Fenton and photo-assisted electro-Fenton, J. Electroanal. Chem. 681 (2012) 36.
[36] A. El-Ghenymy, N. Oturan, M.A. Oturan, J.A. Garrido, P.L. Cabot, F. Centellas, R.M. Rodríguez, E. Brillas, Comparative electro-Fenton and UVA photoelectro-Fenton degradation of the antibiotic sulfanilamide using a stirred BDD/air-diffusion tank reactor, Chem. Eng. J. 234 (2013) 115.
[37] M. Zarei, A.R. Khataee, R. Ordikhani-Seyedlar, M. Fathinia, Photoelectro-Fenton combined with photocatalytic process for degradation of an azo dye using supported TiO_2 nanoparticles and carbon nanotube cathode: Neural network modeling, Electrochim. Acta 55 (2010) 7259.
[38] A. Khataee, A. Khataee, M. Fathinia, B. Vahid, S.W. Joo, Kinetic modeling of photoassisted-electrochemical process for degradation of an azo dye using boron-doped diamond anode and cathode with carbon nanotubes, J. Ind. Eng. Chem. 19 (2013) 1890.
[39] K. Cruz-González, O.A. Torres-Lopez, M. García-León, E. Brillas, A. Hernández-Ramírez, J.M. Peralta-Hernández, Optimization of electro-Fenton/BDD process for decolorization of a model azo dye wastewater by means of response surface methodology, Desalination 286 (2012) 63.
[40] E. Isarain-Chávez, C. de la Rosa, L.A. Godínez, E. Brillas, J.M. Peralta-Hernández, Comparative study of electrochemical water treatment processes for a tannery wastewater effluent, J. Electroanal. Chem. 713 (2014) 62.
[41] S. Garcia-Segura, E. Brillas, Mineralization of the recalcitrant oxalic and oxamic acids by electrochemical advanced oxidation processes using a boron-doped diamond anode, Water Res. 45 (2011) 2975.
[42] E. Guinea, J.A. Garrido, R.M. Rodríguez, P.-L. Cabot, C. Arias, F. Centellas, E. Brillas, Degradation of the fluoroquinolone enrofloxacin by electrochemical advanced oxidation processes based on hydrogen peroxide electrogeneration, Electrochim. Acta 55 (2010) 2101.
[43] H. Zhang, Y. Li, X. Zhong, X. Ran, Application of experimental design methodology to the decolorization of Orange II using low iron concentration of photoelectro-Fenton process, Water Sci. Technol. 63 (2011) 1373.
[44] E. Isarain-Chávez, J.A. Garrido, R.M. Rodríguez, F. Centellas, C. Arias, P.-L. Cabot, E. Brillas, Mineralization of metoprolol by electro-Fenton and photoelectro-Fenton processes, J. Phys. Chem. A 115 (2011) 1234.
[45] L.C. Almeida, S. Garcia-Segura, C. Arias, N. Bocchi, E. Brillas, Electrochemical mineralization of the azo dye Acid Red 29 (Chromotrope 2R) by photoelectro-Fenton process, Chemosphere 89 (2012) 751.
[46] E. Brillas, M.A. Baños, S. Camps, C. Arias, P.L. Cabot, J.A. Garrido, R.M. Rodríguez, Catalytic effect of Fe^{2+}, Cu^{2+} and UVA light on the electrochemical degradation of nitrobenzene using an oxygen-diffusion cathode, New J. Chem. 28 (2004) 314.
[47] M. Stylidi, D.I. Kondarides, X.E. Verykios, Pathways of solar light-induced photocatalytic degradation of azo dyes in aqueous TiO_2 suspensions, Appl. Catal. B: Environ. 40 (2003) 271.
[48] D. Vogna, R. Marotta, A. Napolitano, M. d'Ischia, Advanced oxidation chemistry of paracetamol. UV/H_2O_2-induced hydroxylation/degradation pathways and 15 N-aided inventory of nitrogenous breakdown products, J. Org. Chem. 67 (2002) 6143.